# Smooth landscape solvent dynamics in electron transfer reactions

Vitor B. P. Leite

**Articles you may be interested in**

The energy landscape for solvent dynamics in electron transfer reactions: A minimalist model
J. Chem. Phys. **117**, 2172 (2002); 10.1063/1.1488588

Fractional power dependence of mean lifetime of electron transfer reaction on viscosity of solvent
J. Chem. Phys. **111**, 2665 (1999); 10.1063/1.479542

An ab initio study of specific solvent effects on the electronic coupling element in electron transfer reactions
J. Chem. Phys. **109**, 7414 (1998); 10.1063/1.477403

Electron transfer reaction dynamics in non-Debye solvents
J. Chem. Phys. **109**, 2325 (1998); 10.1063/1.476800

Dwell time of nonadiabatic electron transfer reaction: Solvent dynamic effects
J. Chem. Phys. **107**, 9361 (1997); 10.1063/1.475233

# Smooth landscape solvent dynamics in electron transfer reactions

Vitor B. P. Leite[a]

*Departamento de Física—IBILCE, Universidade Estadual Paulista, São José do Rio Preto 15054-000, SP, Brazil*

Solvent effects play a major role in controlling electron–transfer reactions. The solvent dynamics happens on a very high-dimensional surface, and this complex landscape is populated by a large number of minima. A critical problem is to understand the conditions under which the solvent dynamics can be represented by a single collective reaction coordinate. When this unidimensional representation is valid, one recovers the successful Marcus theory. In this study the approach used in a previous work [V. B. P. Leite and J. N. Onuchic; J. Phys. Chem. **100**, 7680 (1996)] is extended to treat a more realistic solvent model, which includes energy correlation. The dynamics takes place in a smooth and well behaved landscape. The single shell of solvent molecules around a cavity is described by a two-dimensional system with periodic boundary conditions with nearest neighbor interaction. It is shown how the polarization-dependent effects can be inferred. The existence of phase transitions depends on a factor $\gamma$ proportional to the contribution from the two parameters of the model. For the present model, $\gamma$ suggests the existence of ''weak kinetic phase transitions,'' which are used in the analysis of solvent effects in charge–transfer reactions. © *1999 American Institute of Physics.* [S0021-9606(99)50420-0]

## I. INTRODUCTION

Electron transfer (ET) reactions play a major role in many chemical and biological processes,[1,2] in which the solvent effects have been extensively studied.[3–5] The Marcus theory has successfully explained the solvent role in ET by a single collective reaction coordinate.[6] On a different approach to the problem, the solvent dynamics happens on a very high-dimensional surface, and this complex landscape is populated by a large number of minima.[7] One can wonder how this complex landscape view can be accommodated with the single-coordinate picture. This question has been addressed by Onuchic and Wolynes (OW),[8] with a simple model for a polar solvent interacting with a charged cavity representing the donor or acceptor site for ET. Although this model is far from representing details of real solvents, it includes the basic features of a rough-energy landscape: multidimensional degrees of freedom, with each solvent molecule being treated independently; a disordered energy landscape with multiple minima; and a polarizable medium around a charged cavity. Above the thermodynamic glass transition, it recovers the continuum dielectric limit. Recently the dynamics of OW model was studied by Leite and Onuchic,[9] who showed that at high temperatures, the system exhibits effective diffusive one-dimensional dynamics, where the Born–Marcus limit is recovered. At low temperatures, a polarization-dependent glassy phase (*polarization-dependent phase transition*) appears and a slow non-self-averaging dynamics is expected.

The representation of this complex system in terms of a single reaction coordinate resembles the protein folding system. The energy landscape, with the interplay of roughness and driving forces, plays a crucial role controlling the kinetics and thermodynamics of the folding process.[10,11] The solvent problem is a much simpler one, but its understanding in terms of a single reaction coordinate can bring an insight to the protein folding area.

There are several different dynamic regimes in ET systems: adiabatic, nonadiabatic and Zusman's; all of them assuming the existence of a single reaction coordinate which represents the outer-sphere effects. An extensive presentation and discussion of electron transfer reactions controlled by solvent dynamics can be found elsewhere.[3,12,13] If this assumption is not valid, all the above regimes are inadequate, and have to be reevaluated. The OW model addresses the limits of validity of the unidimensional representation. In the previous works[8,9] it was pointed out that the main pitfall of the OW model was the assumption of solvent random energies, i.e., it does not include energy correlation between states. In this work, the simple model is adapted to include energy correlation. The single shell of solvent molecules around a cavity is described by a two-dimensional (2D) system with periodic boundary conditions with nearest neighbor interaction (NNI). The energy landscape is very smooth compared with the random energies case, which leads to a more well behaved type of solvent.

The organization of this paper is as follows. In Sec. II we review the OW model for a solvent,[8] the phase transitions and the high-temperature limit.[9] In Sec. III we discuss the kinetic behavior at low temperatures. The phase transitions are studied using the variables from the previous work.[9] Since very little can be done analytically, the analysis is made mostly by comparing its results with the simpler case, where there is no correlation between energies. In Sec. IV we summarize the results and comments upon their relation with real solvents.
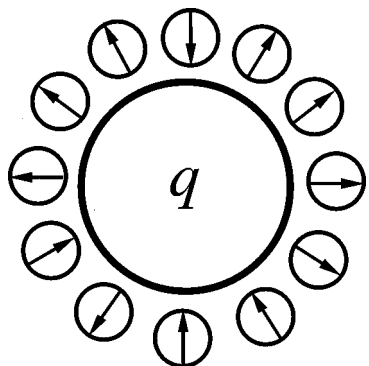
[a]Electronic mail: vleite@df.ibilce.unesp.br

FIG. 1. The single-shell OW model for solvent dipoles around a cavity with charge $q$.

## II. THE SOLVENT MODEL

This model is a minor variation of the thermodynamic Onuchic and Wolynes (OW) solvent model,[8] and the analysis of its dynamics employs the same approaches used earlier.[9] The OW model considers a single shell of solvent molecules with simple rotational dynamics, represented by dipoles pointing only in two directions, inward and outward, i.e., as Ising spins (Fig. 1). The interaction energy between dipoles and between each dipole and the charge cavity are assumed to be rather simple. For the single shell of $N$ dipoles, the solvation energy is

$$E_{solv} = -\sum_{i=1}^{N} \xi_i(q)\sigma_z(i) + \sum_{\langle ij \rangle} J_{ij}\sigma_z(i)\sigma_z(j), \tag{1}$$

where the first term is the dipole–charge interaction and the second term is due to dipole–dipole interaction. $q$ is an index associated to the charge cavity. The charge–dipole interaction $\xi_i(q)$ and the dipole–dipole interaction $J_{ij}$ are assumed to obey a Gaussian distribution, with averages $\bar{\xi}(q)$ and $\bar{J}$ and standard deviation $\Delta\xi(q)$ and $\Delta J$, respectively. Each dipole interacts with only $z$ neighboring dipoles. The total polarization $p$ is defined by

$$p = n_+ - n_-, \tag{2}$$

and

$$n_+ + n_- = N, \tag{3}$$

where $n_+$ ($n_-$) is the number of dipoles oriented inwards (outwards) to the charge cavity. $p$ is used as the reaction coordinate for the solvent, and the free energy depending parametrically on $p$ is used as the effective potential.

The average solvent energy is

$$\bar{E}(x) = N\left[ x\bar{\xi}(q) + \frac{z\bar{J}x^2}{2} \right], \tag{4}$$

where $x = p/N$ is the average polarization per dipole.

The OW model uses the Random Energy Model (REM) approximation[14,15] to evaluate the solvent energies given by Gaussianly distributed random variables. The standard deviation of the solvation energy is assumed independent of $x$,

$$\Delta E^2 = N\Delta\epsilon^2 = N\left[ \Delta\xi^2 + \frac{z\Delta J^2}{2} \right]. \tag{5}$$

The energy probability distribution $g(x,E)$ at polarization $x$ is

$$g(x,E) = \frac{1}{\sqrt{2\pi}\Delta E} \exp\left[ -\frac{(E - \bar{E}(x))^2}{2\Delta E^2} \right]. \tag{6}$$

In the present model, the energies are not simple random variables, but a sum of them, following strictly Eq. (1). The motivation to work with a 2D Ising model with NNI lies in its simple way to introduce energy correlation between states. Our primary goal is to check its behavior with the approach used to investigate the OW model based on REM. What is new in this work is the idea of representing the influence of a disordered system in terms of a single reaction coordinate, which is not addressed in rigorous 2D Ising studies.[16,17] However at the present time we do not know how to correlate the rigorous results with our present work.

For the sake of simplicity, in our simulations the single shell model with NNI is approximated by a 2D lattice with NNI and periodic boundary conditions. Even though this approximation corresponds to a topology of a torus, one can think of it as a topologically distorted spherical shell, where all dipoles have the same coordination number (number of nearest neighbor). In other words, it can be thought as a representation of a "sphere" where the two poles have the same coordination number as all other points. This approximation greatly simplifies the analysis and the computational work without affecting the quantitative results.

While studying the dynamics, in order to define the model completely, one needs to define the way by which the system is allowed to move from one state to another, i.e., the kinetic rules. It allows only a single dipole flip per elementary move, with move acceptance based on a Monte Carlo procedure. That is equivalent to a rate from a state $A$ to a connected state $B$ of

$$R = \begin{cases} \dfrac{R_0}{N}\exp[-(E_B - E_A)/T], & \text{for } E_B > E_A, \\[2ex] \dfrac{R_0}{N}, & \text{for } E_B < E_A, \end{cases} \tag{7}$$

where $R_0$ is associated to the flipping rate of any dipole.

Most real solvents do not present phase transitions at its liquid phase, nevertheless, it is observed a deviation from continuous models at low temperatures.[18] These changes in their dynamics we refer to as kinetic or dynamic phase transitions. In this, sense our model tries to represent the same features of experimental systems. There are three kinetic phase transitions, each of them is associated with a different entropic contribution, which yields to different transition temperatures. The phase transitions are briefly explained below.[9] Though the REM approximation is not valid, we still use it as a qualitative guide in this work.

### A. The phase transitions

#### 1. Polarization-dependent phase transition

The system is studied parametrically on $x$. The entropic relevant number is the number of states with polarization $x$,

$$\Omega(Nx) = \frac{N!}{n_+! n_-!} = \frac{N!}{[N(1-x)/2]! [N(1+x)/2]!}. \qquad (8)$$

The average number of states with polarization $x$ and energy between $E$ and $E + dE$ is

$$\langle n(x,E) \rangle = \Omega(Nx) g(x,E) dE. \qquad (9)$$

Using the REM procedure,[14] for $\langle n(x,E) \rangle \gg 1$, one can approximate $\langle \log n(x,E) \rangle$ by $\log\langle n(x,E) \rangle$, and the entropy becomes

$$S(x,E) \simeq \log\langle n(x,E) \rangle \simeq \log \Omega(Nx) - \frac{(E - \bar{E}(x))^2}{2\Delta E^2}. \qquad (10)$$

At the critical energy,

$$E_c(x) = \bar{E}(x) - \Delta E (2 \log \Omega(Nx))^{1/2}, \qquad (11)$$

the entropy vanishes, and the approximation above is not valid. The system becomes frozen into a small nonexponen-

tial number of states with low energies. In the thermodynamic limit for $E < E_c(x)$, instead of Eq. (10), $S(x,E) = 0$.

For every polarization $x$ there is a critical temperature, the *polarization-dependent phase transition* $T_c(x)$, given by

$$\beta_c(x) = \frac{1}{T_c(x)} = \frac{\partial S}{\partial E}\bigg|_{E = E_c(x)} = \frac{[2 S^*(Nx)]^{1/2}}{\Delta E}, \qquad (12)$$

where $S^*(Nx) = \log \Omega(Nx)$ is the configuration entropy. In the small-$x$ limit,

$$\beta_c(x) = \frac{(2 \log 2 - x^2)^{1/2}}{\Delta \epsilon}. \qquad (13)$$

At a particular $T$, such that $T = T_c(x_0)$, for $|x| < |x_0|$ the system has a behavior like the standard Born–Marcus model. As it hits $x_0$, the dynamics becomes glassy. The average free energy is

$$F(x) = \begin{cases} \bar{E}(x) - \Delta E^2(q)/2T - T S^*(Nx), & \text{for } T > T_c(x) \quad (|x| < |x_0|), \\ E_c(x) = \bar{E}(x) - \Delta E (2 S^*(Nx))^{1/2}, & \text{for } T \leq T_c(x) \quad (|x| > |x_0|). \end{cases} \qquad (14)$$

The free energy, depending parametrically on the total polarization, is used as a smooth effective potential above $T_c(x)$.

### 2. Global phase transition

Thermodynamically, there is only one phase transition, here called the *global phase transition*, which is associated with the total number of states $2^N$. The REM procedure to estimate the entropy, following Eq. (10), is used again, being characterized by

$$S^g(E) = \log[2^N g(E)], \qquad (15)$$

where $S^g(E)$ is the total entropy, and $g(E)$ is the energy probability distribution. Using Eqs. (6) and (12),

$$\beta_c^g = \frac{1}{T_c^g} = \frac{[2N \log 2]^{1/2}}{\Delta E} = \frac{(2 \log 2)^{1/2}}{\Delta \epsilon}, \qquad (16)$$

which is the same result as for $\beta_c(x = 0)$. The critical energy $E_c^g$ where the entropy of the entire system becomes zero, is given by

$$E_c^g = -N \Delta \epsilon (2 \log 2)^{1/2}. \qquad (17)$$

### 3. Local phase transition

This transition is related to the local configurational entropy and local energy distribution of states, corresponding to a temperature where the system starts to get trapped in local minima, $T_c^{loc}$ ($1/\beta_c^{loc}$). Below this temperature, escapes from local minima go preferentially through the neighbor with the smallest barrier instead of overcoming a typical barrier. This phase transition has to do with the conditions under which the system gets trapped in local minima. The deriva-

tion of the local phase transition is obtained via the REM approach used above. If each state is connected with $M$ other states by one elementary move, the average number of neighboring states $\langle n_l(E) \rangle$ for a given state with an energy between $E$ and $E + dE$ is

$$\langle n_l(E) \rangle = \frac{M}{\sqrt{2\pi}\Delta\epsilon_l} \exp\left[-\frac{E^2}{2\Delta\epsilon_l^2}\right] dE, \qquad (18)$$

where $\Delta\epsilon_l$ is the standard deviation of the energy distribution associated with states connected by single-flip kinetics (instead of $\Delta E$ as for REM).

If $\langle n_l(E) \rangle \gg 1$, the local entropy can be approximated by

$$S_l(E) \simeq \log\langle n_l(E) \rangle \simeq \log M - \frac{E^2}{2\Delta\epsilon_l^2}. \qquad (19)$$

There is a critical energy $E_c^{loc}$, where the entropy vanishes $[E_c^{loc} = -\Delta\epsilon_l(2 \log M)^{1/2}]$ and

$$\beta_c^{loc} = \frac{1}{T_c^{loc}} = \frac{\partial S_l}{\partial E}\bigg|_{E = E_c^{loc}} = \frac{(2 \log M)^{1/2}}{\Delta\epsilon_l}. \qquad (20)$$

For $\beta \gtrsim \beta_c^{loc}$ the system spends most of the time at local minima, and the local phase transition is determined only by the local distribution of energies. When the energies between states are correlated, as one changes the state of a single dipole, the total solvation energy changes only by the energy interaction of the flipped dipole with the rest of the system. This difference implies significant changes in the dynamical behavior.

The global and polarization-dependent phase transitions depend on the distribution of energies of the entire system,

$\Delta E$, which are the same as in the REM case.[9] Differently from the random energies case, where the $\beta_c^{loc(REM)}$ is the first transition felt by the system [$\beta_c^{loc(REM)} < \beta_c(x) < \beta_c^g$], now

$$\beta_c(x) < \beta_c^g < \beta_c^{loc}, \tag{21}$$

since for typical values of $M$ ($\sim N$) and $\Delta\epsilon_l \sim \Delta\epsilon$,

$$\frac{(2\log 2 - x^2)^{1/2}}{\Delta\epsilon_l} < \frac{(2\log 2)^{1/2}}{\Delta\epsilon} < \frac{(2\log M)^{1/2}}{\Delta\epsilon}.$$

## B. High-temperature limit

This limit has been discussed in detail in the previous work.[9] The only difference between that work and the present one is the type of interactions, which is irrelevant at this limit. So all the conclusions with respect to high-temperature regimes are applicable to the present model, as follows. The multidimensional master equation can be reduced into a unidimensional diffusion equation for the total polarization. The resulting dynamics corresponds to a particle diffusing in an effective (almost) quadratic potential. In this limit (noninteracting dipoles), all *diffusion paths* are *equivalent* and the unidimensional equation is exact. The free energy, depending parametrically on the total polarization, accurately describes the kinetic effective potential.

## III. LOW TEMPERATURES—SYSTEM WITH INTERACTIONS

In this section dipole–dipole or charge–dipole interactions are considered. For simplification, we discuss only the dipole-dipole interaction, but the general form of interaction can be trivially derived, as it only includes an extra term in $\bar{E}(x)$ [Eq. (4)] and in $\Delta E$ [Eq. (5)]. To probe the different dynamical regimes, we vary the two parameters that characterize the energy distribution, i.e., the average energy of the dipole–dipole interaction, $\bar{J}$, and its random fluctuation with width $\Delta J$. There are two limit cases to be studied.

(a) $\Delta J \neq 0$ and $\bar{J} = 0$. There is no correlation between polarization $x$ and energy. States for all $x$'s obey the same energy distribution.

(b) $\Delta J = 0$ and $\bar{J} \neq 0$. There is no disorder in the interactions.

We first discuss case (a) above. In Sec. III A the *global* and *local* phase transitions are studied. In Sec. III B we discuss the polarization-dependent phase transition. In Sec. III C we investigate case (b). In Sec. III D we address the general case where $\Delta J \neq 0$ and $\bar{J} \neq 0$. The approach used in this section is the same of previous work;[9] the variables observed are the same, so we suggest to the reader to analyze both works together. The previous results are important for a clear understanding of these physical processes. Strictly speaking, there is no phase transition, but some qualitative changes in the dynamics of the system at low temperatures. Even though it is hard to estimate the diffusion coefficient, representing the problem in terms of a single reaction coordinate for the solvent is still possible.
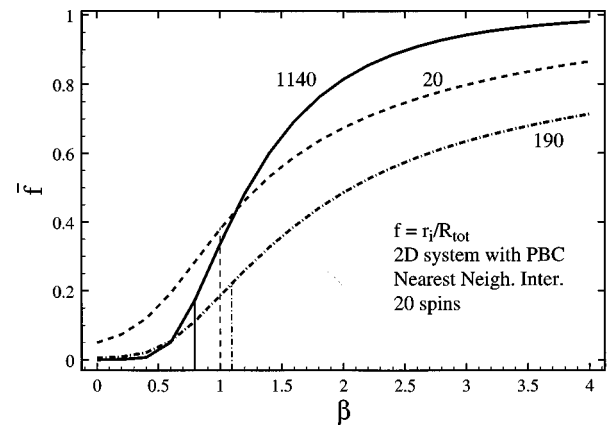


FIG. 2. The average fraction $\bar{f}$ between the fastest neighboring escape rate and the total escape rate [Eqs. (22) and (23)], as a function of the inverse of temperature $\beta$. The system has $\Delta\epsilon = 2$ and 20, 190, and 1140 neighboring states. The vertical lines indicate the position where $\bar{f}$ changes curvature, defined as $\beta_c^{loc}$.

## A. Local and global phase transitions

In this limit, there is no correlation between polarization ($x$) and energy, and states for all $x$'s obey the same energy distribution. Rigorously, a 2D system with a nearest-neighbor interaction does not present a thermodynamic phase transition.[17] The REM approach to estimate the temperature phase transition is valid only for random (noncorrelated) energies. Nevertheless, we still use this approach to have an idea of the dynamics. We do not expect to observe an obvious phase transition in our simulation, as it is observed in the REM case, and indeed the phase transitions observed in this work are "weak kinetic" ones. In this context, the global phase transition corresponds to the weak kinetic polarization-dependent phase transition at $x = 0$. If this simple model is extended to multishell solvent molecules around a cavity, which corresponds to the three-dimensional NNI of Ising spins, then the true global (thermodynamic) phase transition is expected.[17]

The local phase transition is studied, as in Ref. 9, by probing the ratio between rates and the escape times as a function of $\beta$. We compute the ratio $f_i$ between the fastest individual rate to escape from a state $i$ $r_i^{max}$ [$= \max(r_{ij})$] and the total rate $R_i$ of Eq. (7),

$$f_i = r_i^{max}/R_i. \tag{22}$$

The ratio $f_i$ shows the importance of the fastest rate (smallest barrier) on the overall escape rate. When the fastest rate starts to dominate, a single "kinetic" route becomes preferential. To probe this transition, we measure the average value of $f_i$,

$$\bar{f} = \sum_i f_i \exp[-\beta E_i] \Big/ \sum_i \exp[-\beta E_i]. \tag{23}$$

Figure 2 shows $\bar{f}$ for three different systems, with $\Delta\epsilon_l = 4^{1/2}, 8^{1/2}$ and $12^{1/2}$ having $M = 20$, 190 and 1140, respectively (it corresponds to a flip of 1, 2 and 3 dipoles simultaneously, respectively).[19] We average $\bar{f}$ over a sample of 10 systems (for $M = 1140$ one sample only). The phase transi-

TABLE I. Local phase transition $\beta_c^{loc}$ results; the NNI case.

| $M$ neighbor states | Theory $\beta_c^{loc}$ | Simulation $\beta_c^{loc}$ |
|---|---|---|
| 20 | 1.22 | 0.8 |
| 190 | 1.14 | 1.1 |
| 1140 | 1.08 | 1.0 |

tion is very weak, and there is no unique way to define the transition temperature. $\beta_c^{loc}$ is defined as the inflection point for $\bar{f}$. In the ideal phase transition $\bar{f}$ goes from a low to a large value in a small interval of $\beta$, i.e., the second derivative of $\bar{f}$ is large, and the inflection point is meaningful. The meaning of this transition is that below this temperature, escapes from local minima go preferentially through the neighbor with the smallest barrier instead of overcoming a typical barrier. In the NNI case, this transition is very smooth, indicating that ''preferential kinetic'' routes do not play an important role.

Table I compares the local phase transition temperatures obtained through simulation with the infinite limit analytical result given by Eq. (20). Even for such a small system, our kinetic definition is in qualitative agreement with the prediction, specially for a large number of neighbors.

One way of probing the local and global phase transitions is by studying the average and standard deviation of escape times, $\langle t_{esc} \rangle$, $\langle \log t_{esc} \rangle$ and $\Delta \log_{10} t_{esc}$, the same parameters used in Ref. 9. Figure 3 shows these parameters as a function of $\beta$, for 10 different runs, each with $10^4$ escapes for a system with 100 dipoles. Even though the number of escapes (states) probed in this simulation is much smaller than the total number of states in the systems, this is much larger than any number of escapes involved in the mean first passage times (MFPT) that we investigate in the next section ($\sim 10^3$). Runs differ only by the initial conditions. $\beta_c^{loc} = 1.5$ according to Eq. (20), and $\beta_c^g \simeq 1.0$ according to Eq. (16). For $\beta > 1.0$, fluctuations become significant, and the results vary depending on the initial conditions. However, this dependence is much weaker than the random energy case (Fig. 7 in Ref. 9), but it provides qualitative evidence for the weak local and global phase transitions. One should note the fluctuations are very small, compared with the average values.

The results depend on the sample used, but this effect is minimized by increasing the system size, which points to a finite size effect. Once the system is chosen, there is a stronger initial condition dependence as the size of the system is increased.

A true phase transition, like the global phase transition observed in the REM case, is not observed in this 2D Ising system. Even though $\bar{f}$ and $t_{esc}$ qualitatively show the same behavior observed as in the REM case, they happen in a very smooth way. As a consequence, one does not expect to have breakdown of the single reaction coordinate representation.
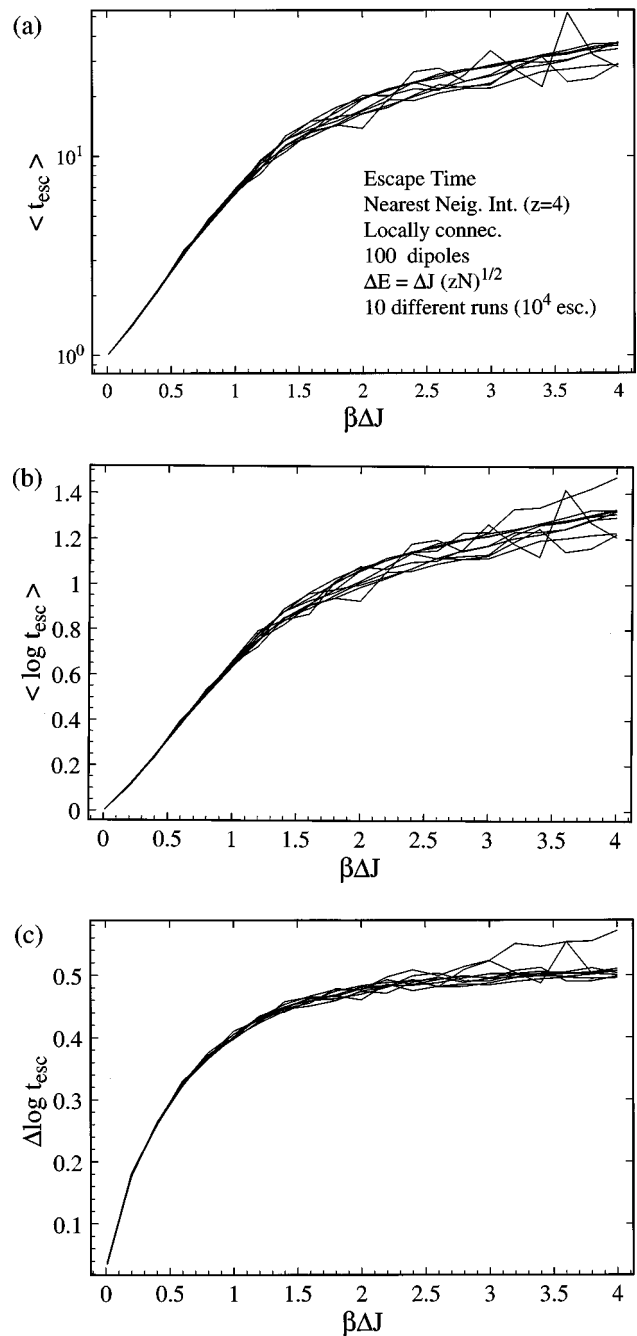


FIG. 3. Escape times on a system with 100 dipoles averaged over $10^4$ escapes as a function of the inverse of temperature (in units of disorder energy parameter $\Delta J$). 10 runs were performed with different annealed initial conditions, using a kinetic scheme where a single dipole flip is allowed ($M = 100$). (a) Average escape time $\langle t_{esc} \rangle$. (b) Average of the log of the escape time $\langle \log t_{esc} \rangle$. (c) Standard deviation of the log of the escape time $\Delta \log t_{esc} = [\langle \log^2 t_{esc} \rangle - \langle \log t_{esc} \rangle^2]^{1/2}$.

## B. Polarization-dependent phase transition

Since $\beta_c(x) < \beta_c^g < \beta_c^{loc}$, as the temperature is lowered, the first dynamic phase transition observed is the polarization-dependent one. In this sub-section we focus on the time evolution of the polarization coordinate. All results are from numerical simulations. Since we are interested in the evolution between two different polarizations, the First Passage Time (FPT) is the characteristic time to describe the

events in the total polarization space. The FPT is defined as the time to evolve from an initial state of polarization $x_i$ to a final $x_f$, $\tau(x_f, x_i)$, from whose distribution all dynamical information can be obtained. We define the stochastic variable $\omega(x_f, x_i)$ as the number of escapes during the evolution between $x_i$ to $x_f$ (the equilibrium polarization is taken as $x_i = 0$). Notice that the number of escapes is different from the number of steps (time), since only successful attempts are considered. For a free random walk, the FPT is given by $\omega_{rw}(x_f, x_i)$, and every step is "successful," with the random walk mean FPT ($\langle \tau(x_f, x_i) \rangle$) being simply the average $\langle \omega_{rw}(x_f, x_i) \rangle$. As the temperature is lowered, since it takes longer for escapes to occur, $\langle \tau(x_f, x_i) \rangle$ increases. For $\beta$ smaller than any critical temperature, the paths are equivalent, and $\langle \tau(x_f, x_i) \rangle$ is simply the product of the average number of escapes and the average escape time,

$$\langle \tau(x_f, x_i) \rangle = \langle \omega_{rw}(x_f, x_i) \rangle \langle t_{esc} \rangle. \quad (24)$$

As $\beta \gtrsim \beta_c$, the system escapes preferentially through some particular neighbors. If it leads to large fluctuations, the paths are not equivalent and $\tau(x_f, x_i)$ deviates from Eq. (24).

In the previous section it was shown that the fluctuations for this model on the escape times are small, so there is no breakdown on the equivalent diffusion pathways picture and on the single reaction coordinate representation. Equation (24) could be written as[20,21]

$$\langle \tau(x_f, x_i) \rangle = \int_{x_i}^{x_f} dx \int_{x_i}^{x} dx' \, \frac{\exp[\beta(F(x) - F(x'))]}{D}, \quad (25)$$

where $F(x)$ is the free energy and $D$ the diffusion constant. Since $\bar{J} = 0$, there is only the entropic term in the free energy, $\beta F(x)$ is not temperature dependent, so the changes in $\tau(x_f, x_i)$ are due to $D$. The effect of the polarization-dependent kinetic transition is manifested through changes in $D$ along the coordinate $x$. Since $D$ is inversely proportional to $\langle t_{esc} \rangle$,[9] the temperature dependence on $t_{esc}$ can be isolated, and the changes on $D$ can be investigated studying $\omega(x_f, x_i)$ as a function of temperature. Because the distribution of $\omega(x_f, x_i)$ is flat, $\langle \log_{10} \omega(x_f, x_i) \rangle$ is calculated instead of $\langle \omega(x_f, x_i) \rangle$. To quantify the deviation from the random-walk result, we calculated

$$\Delta\Omega(x_f, x_i) = \langle \log_{10} \omega(x_f, x_i) \rangle - \langle \log_{10} \omega_{rw}(x_f, x_i) \rangle \quad (26)$$

and

$$\Delta\Psi(x_f, x_i) = \langle \log_{10} \tau(x_f, x_i) \rangle - \langle \log_{10} \omega_{rw}(x_f, x_i) \rangle, \quad (27)$$

as a function of $\beta$, where $\langle \log_{10} \omega_{rw}(x_f, x_i) \rangle$ is the free random-walk result.

We performed simulations on a 30-dipole 2D system with NNI with periodic boundary conditions, calculating 100 FPT for each sample system (on 100 different systems). We are interested in a comparison of different polarizations; Fig. 4 shows $\Delta\Omega(x_f, 0)$ and $\Delta\Psi(x_f, 0)$ as a function of $\beta$ and $x_f$. Because the polarization-dependent phase transition occurs first for large polarizations, $\Delta\Omega(x_f, 0)$ deviates from zero first under these conditions [Fig. 4(a)]. Since the escape times are polarization independent, $\Delta\Psi(x_f, x_i)$ would have the same temperature dependence for all polarizations, Fig. 4(b). Following Eq. (24), $\Delta\Psi(x_f, x_i)$ is proportional to
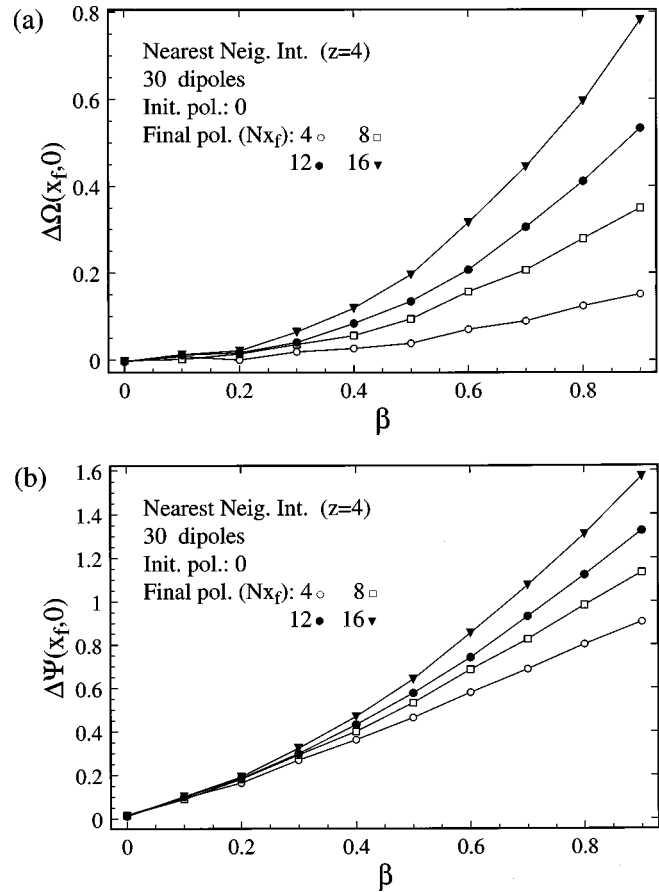


FIG. 4. Evidence for the polarization-dependent phase transition $\beta_c(x)$. (a) $\Delta\Omega(x_f, 0)$ [Eq. (26)], and (b) $\Delta\Psi(x_f, x_i)$ [Eq. (27)] as a function of the inverse of temperature (in units of disorder energy parameter $\Delta J = 1$), $\Delta\epsilon = z^{1/2} = 2$.

$\langle \log_{10} t_{esc}(x_f, x_i) \rangle$, the parameter that should be "physically observable," and one sees the obvious polarization dependence for different curves. The dependence of $\Delta\Psi(x_f, 0)$ with $x_f$s can be interpreted as the variation in the diffusion coefficient in the interval $|x_f|$, and one does not observe a truncated potential, as Onuchic and Wolynes suggested.

## C. Constant dipole–dipole interaction

In this case, there is a nonzero average interaction ($\bar{J} \neq 0$) and no variation in the dipole–dipole interaction ($\Delta J = 0$). The average energy $\bar{E}(x)$ is given by the second term in Eq. (4). For a given polarization $x$ there are different ways $n_+$ "inward" and $n_-$ "outward" dipoles can be arranged, yielding different energies for each $x$. One cannot find a direct analytical form for the energy standard deviation, but this can be calculated for small systems. One expects it to be like

$$\Delta E(x) = \sqrt{\frac{Nz}{2}} \bar{J} \zeta(x), \quad (28)$$

where $Nz/2$ is the number of interactions and $\zeta(x)$ is polarization dependent and has to be calculated from the full enumeration of all states.
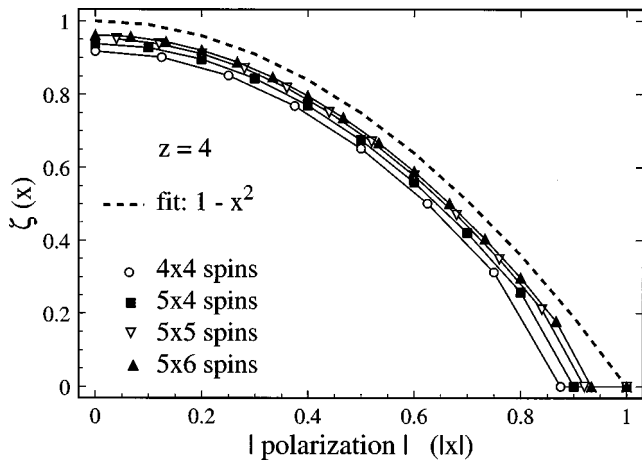
FIG. 5. $\zeta(x)$ for Ising spin dipoles with periodic boundary condition, Eq. (29), in different lattice sizes, and the expected $N$-large limit fit with $1-x^2$.

In Fig. 5, $\zeta(x)$ is shown for systems of $4\times4$, $4\times5$ and $5\times5$ dipoles with periodic boundary conditions. Intuitively, we expect that in the large $N$ limit,

$$\zeta(x) = 1 - x^2, \tag{29}$$

as can be confirmed in Fig. 5.

Now the REM approximation is used to estimate $T_c(x)$, Eq. (12),

$$T_c(x) = \frac{\Delta E(x)}{[2S^*(Nx)]^{1/2}},$$

where $\Delta E(x)$ is given by Eq. (28) and the entropic configuration approximated by[9]

$$S^*(Nx) \simeq N\left[ -\left(\frac{1+x}{2}\right)\log\left(\frac{1+x}{2}\right) - \left(\frac{1-x}{2}\right)\log\left(\frac{1-x}{2}\right) \right]. \tag{30}$$

$T_c(x)$ decreases as $|x|$ increases. In the previous case (Sec. III B), when $\Delta E(x)$ is constant $T_c(x)$ increases with $|x|$. Both behaviors are shown in Fig. 6.
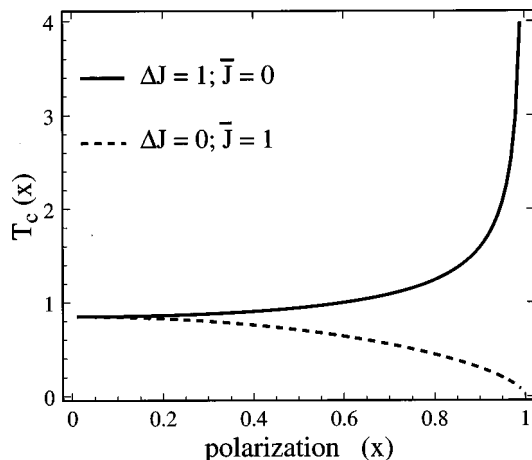


FIG. 6. Polarization-dependent critical temperatures $T_c(x)$ for the two different regimes: (a) $\bar{J}=0$ and $\Delta J \neq 0$ (Sec. III B) and (b) $\bar{J} \neq 0$ and $\Delta J=0$ (Sec. III C).

As discussed in Ref. 9, there are different kinetic regimes when both polarization-dependent average energy $[\bar{E}(x)]$ and roughness ($\Delta E$) are present. These regimes appear according to the relative values of average potential barrier between two polarizations $x_f$ and $x_i$, $\bar{E}(x_f)-\bar{E}(x_i)$ and $\Delta E$. They are measured by the parameter $\gamma$,

$$\gamma(x_f,x_i) = \frac{\bar{E}(x_f)-\bar{E}(x_i)}{\Delta E(x_f)^2/T}. \tag{31}$$

For $x_i=0.0$ and temperatures close to the critical temperatures ($\bar{J}/T \simeq 1$),

$$\gamma(x_f,0) = \frac{x_f^2}{\zeta(x_f)^2} = \frac{x_f^2}{(1-x_f^2)^2}. \tag{32}$$

The phase transitions are expected for $\gamma \ll 1$. Since the landscape is not so rough, by kinetic transitions we mean qualitative changes in $D$, which are polarization-dependent. If one considers that this occurs for $\gamma < 0.1$, then $x_f < 0.3$, which corresponds to polarizations very close to the equilibrium coordinate.

### D. General case $[\bar{E}(x) \neq 0$ and $\Delta E \neq 0]$

For the general case, the roughness is given by

$$\Delta E(x) = \left[ \frac{Nz}{2}(\Delta J^2 + \bar{J}^2 \zeta^2(x)) \right]^{1/2}. \tag{33}$$

The idea is to increase the relative value of $\bar{J}/\Delta J$ and observe how the polarization-dependent diffusion coefficient behaves. If the equivalent path idea is valid, then

$$\tau(x_f,x_i) = \langle \omega_{rw}(x_f,x_i) \rangle \langle t_{esc} \rangle \exp[\beta(\bar{E}(x_f)-\bar{E}(x_i))]. \tag{34}$$

Because of the flat distribution of $\tau(x_f,x_i)$, $\langle \log_{10} t_{esc}(x_f,x_i) \rangle$ is calculated for different values of $\bar{J}/\Delta J$. Taking into account the nonzero average interaction $\bar{E}(x)$ and using Eq. (34),

$$\langle \log_{10} t_{esc}(x_f,x_i) \rangle = \langle \log_{10} \tau(x_f,x_i) \rangle - \langle \log_{10} \omega_{rw}(x_f,x_i) \rangle$$
$$- [\beta(\bar{E}(x_f)-\bar{E}(x_i))] \log_{10} e. \tag{35}$$

The above approximation is valid as long as $\gamma \ll 1$. When the average potential barrier is large compared to the disorder, $D$ depends on the average potential barriers at each $x$, and the comparison of $\langle \log_{10} t_{esc}(x_f,x_i) \rangle$ for different $x_f$ becomes meaningless. $\langle \log_{10} t_{esc}(x_f,x_i) \rangle$ as a function of $\beta \Delta J$ for different $x_f$ and $\bar{J}/\Delta J$ are shown in Fig. 7. For $\bar{J}/\Delta J=0$ ($\gamma =0$) one gets just the result of Fig. 4(b) with stronger $x_f$ dependence as $\beta$ ($1/T$) increases, and the kinetic transitions are expected to approximately follow Fig. 6. For $\bar{J}/\Delta J =0.1$ ($\gamma \lesssim 0.1$) the relative $x_f$ dependence is smaller. Finally, for $\bar{J}/\Delta J=0.3$ ($\gamma \lesssim 0.3$) the disorder becomes less important for the dynamics, and the polarization-dependent effect starts to disappear. The diffusion constant is polarization independent. Gradually one gets back to the previous case ($\bar{J} \neq 0$ and $\Delta J=0$), where even though there is no trivial description of the diffusion dynamics, the unidimensional representation of
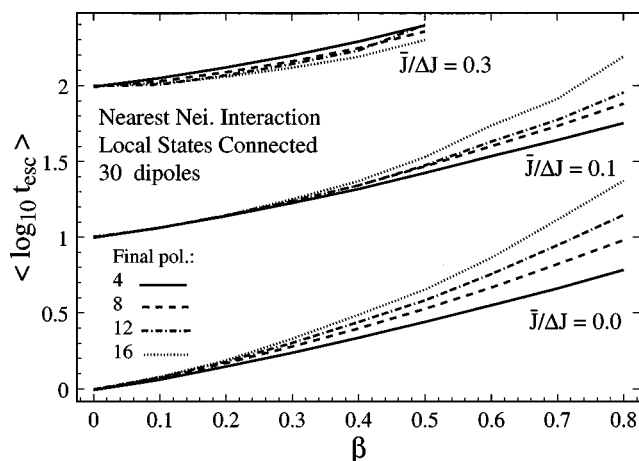
FIG. 7. $\langle \log_{10} t_{esc} \rangle$ according to Eq. (35) for different final polarizations ($Nx_f$) as a function of $\beta$. For $\bar{J}/\Delta J = 0.0$ and 0.1 there is a stronger dependence on $\langle \log_{10} t_{esc} \rangle$ for larger polarizations, in agreement with $T_c(x)$ [Eq. (12)]. For $\bar{J}/\Delta J = 0.3$ the dependence on $Nx_f$ is not well defined.

the problem is expected. There is no breakdown of the reaction coordinate as in Ref. 9, since the diffusion paths are still equivalent.

Even at temperatures below $T_c^{loc}$ (the smallest of the critical temperatures), because the fluctuations on escape times are not large compared with their mean values, the equivalent diffusion paths are still expected. The breakdown of the single reaction coordinate representation occurs rather because the system becomes frozen. At very low temperatures $T \ll T_c^{loc}$, the system is trapped in local minima for longer times, but specially it does not evolve along the $x$ coordinate, for it cannot overcome the average potential energies between polarizations $x_i$ and $x_f$, being effectively frozen.

## IV. CONCLUSION

Electron transfer reactions are strongly controlled by solvent effects. It has been shown, using the OW model, that a complex solvent landscape can be reduced kinetically and thermodynamically into a global one-dimensional reaction coordinate.[9] The biggest pitfall of the OW model is that it does not include energy correlation between states, which is not realistic. In this work, a more realistic system was explored with energy correlation between states, namely of Ising dipoles solvent molecules with nearest-neighbor interaction.

The representation of the solvent by a single reaction coordinate, which validates the Marcus theory for ET, is possible as long as equivalent diffusion paths for the solvent dynamics exist during the solvent dynamical evolution in the polarization coordinate. As the system evolves between two polarization values, it may do it through different paths that, at high enough temperatures, are kinetically equivalent. In this regime, this "complex solvent" shows a Debye-like behavior and the Marcus theory is recovered. As the temperature is lowered, kinetic phase transitions take place and the equivalent path description breaks down. In the present

model there are no real phase transitions. The "weak kinetic transitions" are associated with changes in the diffusion constant, which can be qualitatively observed.

One can imagine for simple solvent models two extreme features. One presents a very rough landscape, like the OW model, with phase transitions and glassy phases. The other one would be a model in a highly organized medium with very little roughness in the landscape. It does not present phase transitions and the single reaction coordinate representation is valid for almost all temperatures, corresponding to the case of Sec. III C. The behavior of intermediate cases were discussed in Sec. III A, III B and III D. The role of the roughness gradually appears in the behavior of the diffusion constant, and as the roughness increases real phase transitions start to appear.

We have shown that the methods of Leite and Onuchic[9] to infer the importance of disorder are adequate. Even when the system has a well behaved smooth landscape, the qualitative changes can be observed. In the 2D NNI solvent case, the landscape is not very rough, the qualitative phase transitions are weak and the unidimensional representation is valid. As the temperature decreases there is a slow down in the dynamics. The description of the system goes from the high-temperature Onuchic–Wolynes limit[8] to low temperature Sumi–Marcus behavior[22] with slow dynamics, down to very low temperatures, when it is completely frozen and follows the Marcus description in frozen media.[23]

The solvent behavior is expected to vary according to the type of interaction (NNI, next-NNI, etc.) and topology (single shell, multiple shell), and of course with the degree of disorder. The essential features are expected to hold more generally in the limiting cases: (1) the high-temperature limit with Marcus-like behavior, and (2) the low-temperature limit with glassy behavior.

From this work the critical temperatures for real solvents can be estimated only with the knowledge of the parameters of our model, the roughness $\Delta E$ and the average polarization-dependent energy $\bar{E}(x)$, which could be calculated via Monte Carlo methods. The functions $\bar{f}$, $t_{esc}$ and the analysis of MFPTs can also be used in all atoms simulations to infer the existence of phase transitions. An interesting study would be to adapt this analysis to probe the relaxation processes on these simple solvent models and in real solvent simulations. It might be possible to address the temperature-dependent solvent relaxation results in ethanol and propanol,[18] where there is a breakdown of continuum theories at low temperatures.

This solvent model, with local interactions and kinetics, behaves in analogy with the protein funnel as a perfect funnel. The connectivity is well behaved[9] and the type of interaction does not provide a very rough landscape. Therefore the studying the relaxation in these systems might help in understanding the relaxation in well behaved protein folding funnels.[24]

## ACKNOWLEDGMENTS

[1] D. D. Vault, *Quantum-Mechanical Tunnelling in Biological Systems* (Cambridge University Press, New York, 1984).

[2] P. F. Barbara, T. J. Meyer, and M. A. Ratner, J. Phys. Chem. **100**, 131–148 (1996).

[3] H. Heitele, Angew. Chem. Int. Ed. Engl. **32**, 359–377 (1993).

[4] R. M. Stratt and M. Maroncelli, J. Phys. Chem. **100**, 12981 (1996).

[5] P. J. Rossky and J. D. Simon, Nature (London) **370**, 263 (1994).

[6] R. A. Marcus and N. Sutin, Biochim. Biophys. Acta **811**, 265 (1985).

[7] V. Daggett and M. Levitt, Annu. Rev. Biophys. Biomol. Struct. **22**, 353 (1993).

[8] J. N. Onuchic and P. G. Wolynes, J. Chem. Phys. **98**, 2218–2224 (1993).

[9] V. B. P. Leite and J. N. Onuchic, J. Phys. Chem. **100**, 7680–7690 (1996).

[10] J. N. Onuchic, Z. Luthey-Schulten, and P. G. Wolynes, Annu. Rev. Phys. Chem. **48**, 539 (1997).

[11] J. D. Bryngelson, J. N. Onuchic, N. D. Socci, and P. G. Wolynes, Proteins: Struct., Funct., Genet. **21**, 167–195 (1995).

[12] K. Yosihara, K. Tominaga, and Y. Nagasawa, Bull. Chem. Soc. Jpn. **68**, 696 (1995).

[13] J. N. Onuchic and P. G. Wolynes, J. Phys. Chem. **92**, 6495 (1988).

[14] B. Derrida, Phys. Rev. Lett. **45**, 79–82 (1980).

[15] B. Derrida, Phys. Rev. B **24**, 2613–2626 (1981).

[16] N. N. Shalaev, Phys. Rep. **237**, 129–188 (1994).

[17] K. Binder and A. P. Young, Rev. Mod. Phys. **58**, 801–976 (1986).

[18] M. Maroncelli, J. Mol. Liq. **57**, 1–37 (1993).

[19] The local energy standard deviation is $\Delta\epsilon_l = \sqrt{z}\Delta J$. In a 2D system with NNI, $z$ is 4; in our simulations we use $\Delta J = 1$, so for a single flip dynamics $\Delta\epsilon_l = 2$.

[20] P. Hänggi, P. Talkner, and M. Borkovec, Rev. Mod. Phys. **62**, 251 (1990).

[21] J. D. Bryngelson and P. G. Wolynes, J. Phys. Chem. **93**, 6902–6915 (1989).

[22] H. Sumi and R. A. Marcus, J. Chem. Phys. **84**, 4894 (1986).

[23] R. A. Marcus, J. Phys. Chem. **94**, 4963 (1990).

[24] M. Skorobogatyy, H. Guo, and M. Zuckermann, Phys. Rev. E **55**, 7354 (1997).